NTU Journal of Engineering and Technology (2025) 4 (2) : 17-23
DOI: https://doi.org/10.56286/ntujet.v4i2

IRAQI Academic Scientific Journals

P-ISSN: 2788-9971 E-ISSN: 2788-998X
NTU Journal of Engineering and Technology
Available online at: https://journals.ntu.edu.iq/index.php/NTU-JET/index

Mapping Clay and Clay Mineral Deposits in Kirkuk City using Landsat Satellite Data

Veyan Farhad Salahalden [1], Muntadher Aidi Shareef [2], Qahtan A.M. Al Nuaimy [2]
[1]Master student at Surveying, Engineering Technical College- Kirkuk, Northern Technical University, Mosul, Iraq
[2,]Surveying, Engineering Technical College- Kirkuk, Northern Technical University, Mosul, Iraq
veyan.farhad@ntu.edu.iq, Muntadher.a.shareef@ntu.edu.iq, qahtaniraqi@ntu.edu.iq

Article Informations

Received: 02-07- 2023,
Revised: 19-08- 2023,
Accepted: 26-08-2023,
Published online: 23-06-2025

Corresponding author:
Name: Veyan Farhad Salahalden
Affiliation: Northern Technical University
Email: veyan.farhad@ntu.edu.iq

Key Words:
Clay,
Remote sensing,
Band ratio,
Band Composite,

A B S T R A C T

The focus of this study is to generate maps of clay and clay mineral deposits in the Kirkuk, Bor, and Jambor structures using Landsat imagery. The authors utilized the band ratio (5/7) and band composite (3,4,5) techniques in their analysis. Fifty-two sites were selected as testing data to evaluate the accuracy of the generated map, which showed a correlation of 0.74. The study concludes that remote sensing techniques provide a cost-effective and accurate means to map the locations of clay and clay mineral deposits, offering an alternative to traditional mapping methods.

1. Introduction

Clay is recognized as a crucial soil characteristic [1, 2]. Under conditions of moderate temperature and high humidity, chemical weathering of carbonate rocks gives rise to the formation of red clay, a residual clay varying in color from brownish yellow to red [3, 4]. The unique physical and chemical properties of clays have found diverse applications in ceramics, construction materials, health, agriculture, civil engineering, the environment, and the chemical industry, dating back to ancient times [5-7]. Traditional soil survey methods are expensive and challenging to implement in remote regions [8-10]. An enormous amount of data on Earth's surface are available via remote sensing images from a broad range of space and airborne sensors, allowing for global and comprehensive evaluation, detection, and monitoring of changes [11-13].Satellite imagery has proven instrumental in soil mapping, as it provides continuous and quantitative measurements of surface reflectance, which are linked to specific soil parameters [2, 8, 9, 14, 15]. Remote sensing offers a broad view of extensive areas, and with the availability of multispectral high-resolution data and advanced digital image processing techniques, it enhances the capability to delineate lithology and geological structures with increased accuracy, offering an integrated and spatial perspective of various land characteristics [16-19]. Considering the importance of investigating soil's physical and chemical properties and predicting these attributes, researchers have employed various techniques [20, 21]. For instance, [17] generated a false-color composite image using band ratios to identify spectral reflectance of mineral deposits. The chemical composition of soil was investigated using gamma and neutron radiation, as well as inductively coupled plasma-mass spectrometry [22]. Remote sensing data has been associated with a wide range of soil characteristics, including particle size distribution and organic substances, using regression analysis models [16, 23-26]. In the study, remote sensing and GIS techniques were employed to identify heavy, light, and clay minerals in Hindiya, Iraq, and the findings demonstrated the usefulness of Landsat images in determining mineral distribution [27]. The Injana and Fatha Formations in Kirkuk cover a substantial area and serve as raw material sources for various industries, including brick production. Conducting research across all formations would be time-consuming and resource-intensive. Therefore, the development of a model for predicting the physical and chemical characteristics of clay and minerals using remote sensing becomes imperative. This research aims to generate maps of clay and clay mineral deposits in the Kirkuk, Bor, and Jambor structures by utilizing band ratio and band composite techniques.

2. Material and Methods

2.1 Location of the study area

The research site is located in the northern region of Iraq, situated between the longitudes 44° 10' and 44° 40' east, and the latitudes 35° 10' and 35° 30' north. The study area covered a land area exceeding 268.12 km^2, encompassing both the Fatha and Injana Formations. The climate of the region is characterized as semiarid and Mediterranean, with hot and dusty summers, and cold winters [28]. The primary period of precipitation occurs between December and March. Please refer to Figure 1 for further details

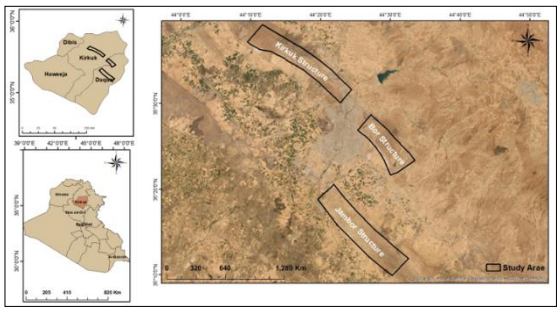

Fig. 1. Location of the study area.

2.2 Soil analysis and data preparation

The methodology employed in this study encompasses field measurements, satellite data, and the application of GIS techniques. Specifically, band ratio and band composite were utilized to investigate the red clay content in the study area. A total of 52 soil sampling sites were selected within the Bor, Jambor, and Kirkuk structures, which are part of the Fatha and Injana Formations. The precise coordinates of these sites were determined using a portable GPS device with an accuracy of ±3.6.

After removing the topsoil layer, soil samples were taken from each site at a depth of 30 centimeters to calculate the red clay content and compare it with the GIS methods. After being exposed to air for drying, these samples were sent to a lab for additional analysis.

In the laboratory, the soil samples underwent tests to determine their particle size using hydrometers. Once the laboratory results were acquired and the satellite image was downloaded, the data were imported into the ArcMap program for further analysis and visualization.

2.3 Preprocessing for satellite images

The quality of aerial and spacecraft views of Earth's surface is significantly impacted by atmospheric conditions, as stated by [29]. The presence of the Earth's atmosphere introduces atmospheric errors, particularly in the delay of GPS signals. To mitigate the effects of scattering and absorption caused by the environment, atmospheric correction is employed to derive surface reflectance characterization (surface properties) [29, 30]. Acquiring precise visuals necessitates a process known as radiometric calibration. Radiometric calibration (radiometric correction) normalizes sensor-collected digital picture data to a reference physical scale using measured reflectance from objects on the ground. [31, 32].

Top-of-atmosphere (TOA) reflectance values are calculated using Landsat 7 multispectral image data, which is represented as quantified and calibrated scaled digital numbers (DN), a model based on USGS-published algorithms is utilized.

Equation 1 is employed to calculate the ToA as per this model

$$R = QM + A \quad (1)$$

where

R= TOA reflectance

Q= Pixel value (digital number)

M= Band- specific multiplicative rescaling factor from the metadata.

A= Band- specific additive rescaling factor from the metadata.

TOA reflectance corrected for the sun angle by using equation 2:

$$TOA\ reflectance\ corrected\ for\ the\ sun\ angle = TOA\ reflectance / \sin(sun\ angle) \quad (2)$$

Following the initial steps, the next phase involves generating a mosaic in ArcMap to cover the entire research area. A region of interest (ROI) is employed to subset a satellite image, and radiometric enhancement techniques are utilized to mitigate the impact of haze.

The regression model is employed to establish strong correlations and calculate the Pearson correlation coefficient (R). To conduct these statistical analyses, the SPSS software version 28 is utilized.

2.4 Band composite

This technology relies on capturing three multi-spectral bands and presenting them within the visible wavelength range, enabling human visual perception. The selection of specific bands is determined by the reflectivity intensity of the target material in each band According to spectral fingerprints for clay derived from the spectral library of the United States Geological Survey (USGS), bands 3, 4, and 5 have a high reflectance. For that, the GIS was used to obtain the composite image by using bands 3, 4, and 5 of the Landsat image. Figure 2, as provided by [33], illustrates the reflectivity curve of the kaolinite mineral according to data published by the US Geological Survey.

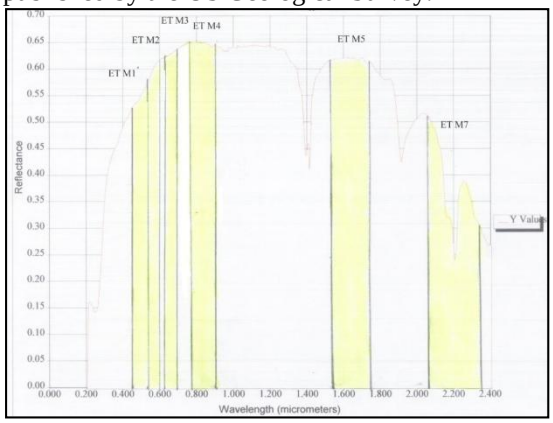

Fig. 2. The reflectivity curve of the mineral kaolinite [33].

2.5 Band ratio

Digital numbers (DNs) from one spectral band are divided by the DNs from another band to produce a ratio image.. These images, known as ratio images, offer enhancements that highlight spectral or color properties of image components, regardless of variations in scene lighting conditions. This feature is a key advantage of ratio images, as it enables the expression of subtle spectral changes that may be concealed by variations in brightness within individual spectral band images or standard color composites. The utilization of ratio images proves particularly useful in distinguishing fine spectral variations within a scene that may otherwise be overshadowed by brightness discrepancies in individual bands or standard color representations [35].

The spectral fingerprints for clay were derived from the spectral library of the United States Geological Survey (USGS). Analysis of Landsat-ETM+ resampled spectra indicates that band 7 has a lower reflectance compared to band 5. Consequently, the use of a shortwave infrared (SWIR) band ratio, specifically the ratio between bands B5 and B7, may be employed as a means to identify and characterize clay minerals.

Band ratio obtained by using equation 3

$$DN_1 = \frac{DNx}{DNy} \quad (3)$$

In the ratio image, where DN_1 represents the numeric value of the image, DNx and DNy denote the numeric values of the numerator and denominator respectively, at the same cell location [33, 35].

The underlying concept of this technique involves dividing bands with high reflectivity by those with

low reflectivity in order to differentiate mineral deposits [33].

In numerous studies, the division of Band 5 by Band 7 has been commonly employed to investigate clay compositions [33, 36-38]. GIS was used to obtain ratio image.

2.6 Validation

The validation approach is used to assess the degree of correlation between the observed and predicted clay content. One particular data point is temporarily excluded from the collection, and the value at that position is then computed based on the remaining data points. The projected value is compared to the actual sample value, which was previously excluded, and can be computed as follows in equation 4:

$$\text{RMSE} = \sqrt{\frac{1}{n}\sum_{i=1}^{n}(Z_i - Z)^2} \qquad (4)$$

where Z is the predicted value and Z_i is the observed value at the sampling point.

3. Results and Discussion

3.1 Soil analysis

The particular size analysis of fifty-two soil samples revealed that gravel comprised the lowest percentage in the majority of samples, ranging from 0 to 4. The results for sediment varied between 0 and 30%. Silt dominated the majority of samples, with concentrations ranging from 28.42% to 93.83%. The clay content ranges from 1.53 to 38.97%.

3.2 Band composites

Utilizing the reflectivity curve provided by the US Geological Survey, the combination of Landsat 7 bands 3, 4, and 5 was employed to visualize the clay content, as clay minerals tend to exhibit high reflectivity in this specific band composite. The regions within the study area that are rich in kaolinite are depicted as purple. The result showed that the clay content was high in the Bor structure compared with the Kirkuk and Jambor structures. And these results agree with the laboratory results, which showed that the percentage of clay in the Bor structure is higher than in the Kirkuk and Jambur structures. Figures 3, 4, and 5 present the outcomes of the band composites for the three respective sections of the study.

3.3 Band ratio

The band ratio technique is based on dividing bands with high reflectivity by those with low reflectivity to accurately detect mineral deposits. Specifically, in the case of identifying kaolinite minerals, bands 5 and 7 were utilized. Band 5 demonstrated a high reflectivity characteristic, whereas band 7 exhibited low reflectivity for kaolinite. The result shown that the upper part of the Bor structure has the highest percentage of red clay, and these results agree with the laboratory results, which showed that the percentage of clay in the upper part of the Bor structure is the highest with 38%. The band ratio results for the three sections are illustrated in Figures 6, 7, and 8. The regions displaying the highest concentration of kaolinite are represented by the color green.

3.4 Validation

A total of fifty-two sites were employed to assess the accuracy of the map, revealing a correlation coefficient of 0.74 between the observed and estimated clay content. In the lab, clay contents ranged from 1.53 to 38.97%, while estimates based on Landsat images ranged between 1% and 30%.This correlation is illustrated in Figure 9.

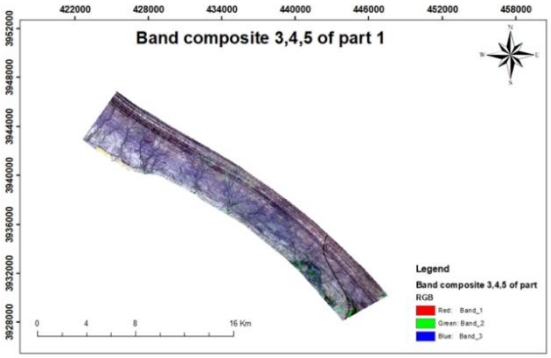

Fig. 3. Band composite in Kirkuk structure.

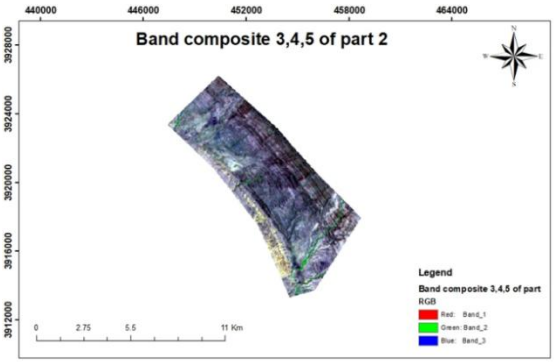

Fig. 4. Band composite in Bor structure.

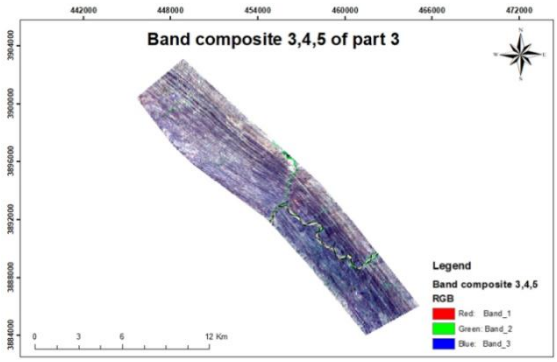

Fig. 5. Band composite in Jambor structure.

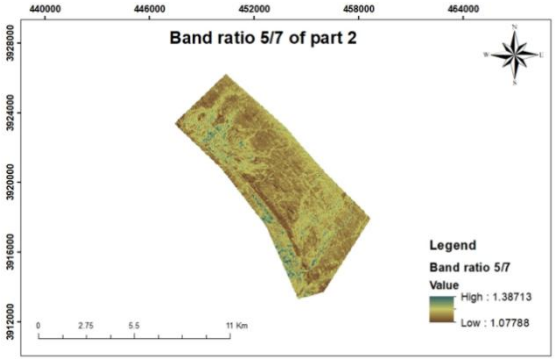

Fig. 6. Band ratio in Kirkuk structure

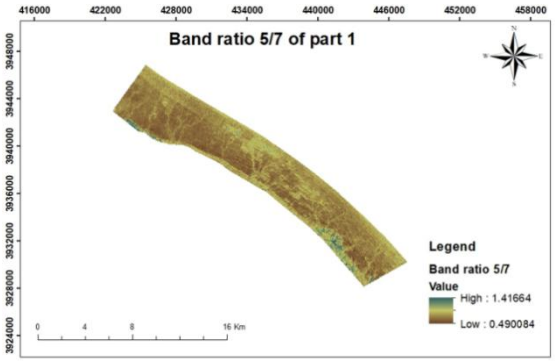

Fig. 7. Band ratio in Bor structure.

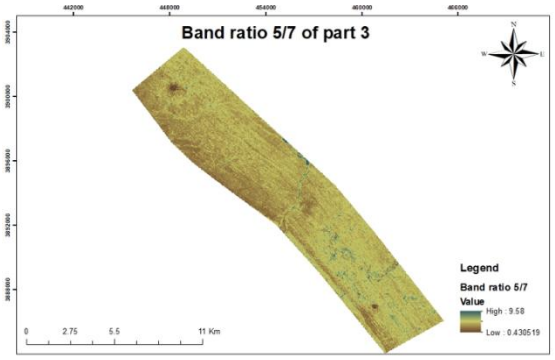

Fig. 8. Band ratio in Jambor structure.

4. Conclusion

The application of Landsat 7 band composites and band ratio techniques demonstrated their effectiveness in the identification and mapping of regions rich in kaolinite within the study area. The visualization of clay content through purple color representations facilitated clear and straightforward identification, enabling convenient analysis. These techniques exhibit promising potential for future research, as they can be utilized to identify various other mineral deposits and contribute to effective resource management strategies.

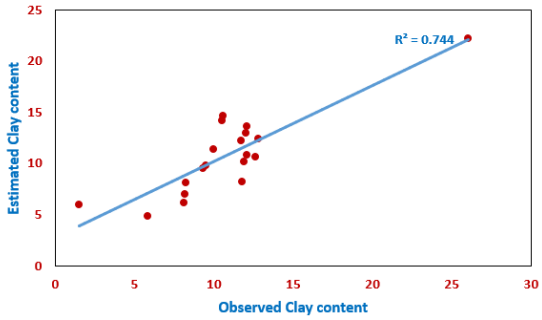

Fig. 9. Correlation between the observed and estimated clay.

Clay content was estimated to be between 1 to 30 using the Landsat image, with a correlation of 0.74%. Samples could not be collected from all of the study regions, which was a major limitation of the research. To obtaining more precise results, would require doing fieldwork at remote sites. Also, use a variety of satellite images to get even more accurate and comprehensive information.

Competing Interests

The authors declare that there are no competing interests.

References

[1] N. R. Ismail and H. M. Omar, "Assessment of some clay deposits from Fatha Formation (M. Miocene) for brick manufacturing in Koya area, NE Iraq," *ARO-The Scientific Journal of Koya University*, vol. 2, no. 1, pp. 16–23, 2014.

[2] M. Shabou *et al.*, "Soil clay content mapping using a time series of Landsat TM data in semi-arid lands," *Remote Sensing*, vol. 7, no. 5, pp. 6059–6078, 2015.

[3] Y. Zhang, S. Pu, R. Y. M. Li, and J. Zhang, "Microscopic and mechanical properties of undisturbed and remoulded red clay from Guiyang, China," *Scientific Reports*, vol. 10, no. 1, p. 18003, 2020.

[4] A. Castrillón *et al.*, "Clay mineralogy and texture of deep-sea hydrothermal mudstone associated with the Cerro Matoso peridotite in accreted oceanic crust from Colombia," *J. South Am. Earth Sci.*, vol. 117, p. 103886, 2022.

[5] J. M. Moreno-Maroto and J. Alonso-Azcárate, "What is clay? A new definition of 'clay' based on plasticity and its impact on the most widespread soil classification systems," *Appl. Clay Sci.*, vol. 161, pp. 57–63, 2018.

[6] A. A. Surdashy and A. M. Aqrawi, "Assessment of Clay Deposits Quality from East of Erbil, Kurdistan Region, Iraq for some Ceramic Industries," *Iraqi Geol. J.*, pp. 145–161, 2021.

[7] M. H. Ali, M. R. Abood, and G. A. Zarraq, "Validity of the Injana Claystones as Fillers Al-Hajaj, Northern Salah-Alddin, Iraq," *Iraqi Geol. J.*, pp. 42–49, 2023.

[8] A. B. McBratney, M. M. Santos, and B. Minasny, "On digital soil mapping," *Geoderma*, vol. 117, no. 1–2, pp. 3–52, 2003.

[9] C. E. Akumu *et al.*, "GIS-fuzzy logic based approach in modeling soil texture: Using parts of the Clay Belt and Hornepayne region in Ontario Canada as a case study," *Geoderma*, vol. 239, pp. 13–24, 2015.

[10] M. Zeraatpisheh *et al.*, "Conventional and digital soil mapping in Iran: Past, present, and future," *Catena*, vol. 188, p. 104424, 2020.

[11] M. A. Shareef, S. F. Hasan, and Q. M. Ajaj, "Estimation and mapping of dates palm using Landsat-8 images: A case study in Baghdad city," in *Proc. Int. Conf. Adv. Sci. Eng. (ICOASE)*, 2018, pp. 425–430.

[12] M. A. Shareef, M. H. Ameen, and Q. M. Ajaj, "Change detection and GIS-based fuzzy AHP to evaluate the degradation and reclamation land of Tikrit City, Iraq," *Geodesy Cartogr.*, vol. 46, no. 4, pp. 194–203, 2020.

[13] S. F. Hasan, M. A. Shareef, and N. D. Hassan, "Speckle filtering impact on land use/land cover classification area using the combination of Sentinel-1A and Sentinel-2B," *Arab. J. Geosci.*, vol. 14, no. 4, p. 276, 2021.

[14] A. G. Gudkov *et al.*, "A portable microwave radiometer for proximal measurement of soil permittivity," *Comput. Electron. Agric.*, vol. 198, p. 107076, 2022.

[15] Y. Yan *et al.*, "High-Resolution Mapping of Soil Organic Matter at the Field Scale Using UAV Hyperspectral Images with a Small Calibration Dataset," *Remote Sens.*, vol. 15, no. 5, p. 1433, 2023.

[16] K. Liao, S. Xu, J. Wu, and Q. Zhu, "Spatial estimation of surface soil texture using remote sensing data," *Soil Sci. Plant Nutr.*, vol. 59, no. 4, pp. 488–500, 2013.

[17] A. K. Martins and B. L. Gadiga, "Satellite remote sensing for mineral deposit assessment of clay in Mubi Local Government Area of Adamawa State, Nigeria," *Geoscience*, vol. 5, no. 1, pp. 26–30, 2015.

[18] H. Shirmard, E. Farahbakhsh, R. D. Müller, and R. Chandra, "A review of machine learning in processing remote sensing data for mineral exploration," *Remote Sens. Environ.*, vol. 268, p. 112750, 2022.

[19] A. Amer, M. Al-hadithi, and M. A. Shareef, "Assessment of Landslide Hazards Using GIS-Based Techniques: An Overview 2000–2020," *NTU J. Renew. Energy*, vol. 4, no. 1, pp. 18–25, 2023.

[20] E. Eyo and S. Abbey, "Multiclass stand-alone and ensemble machine learning algorithms utilised to classify soils based on their physico-chemical characteristics," *J. Rock Mech. Geotech. Eng.*, vol. 14, no. 2, pp. 603–615, 2022.

[21] Z. Ur Rehman, M. F. Junaid, N. Ijaz, U. Khalid, and Z. Ijaz, "Remediation methods of heavy metal contaminated soils from environmental and geotechnical standpoints," *Sci. Total Environ.*, vol. 867, p. 161468, 2023.

[22] A. H. Taqi, Q. A. Al Nuaimy, and G. A. Karem, "Study of the properties of soil in Kirkuk, IRAQ," *J. Radiat. Res. Appl. Sci.*, vol. 9, no. 3, pp. 259–265, 2016.

[23] C. Da Silva Chagas, W. de Carvalho Junior, S. B. Bhering, and B. Calderano Filho, "Spatial prediction of soil surface texture in a semiarid region using random forest and multiple linear regressions," *Catena*, vol. 139, pp. 232–240, 2016.

[24] M. R. Nanni and J. A. M. Demattê, "Spectral reflectance methodology in comparison to traditional soil analysis," *Soil Sci. Soc. Am. J.*, vol. 70, no. 2, pp. 393–407, 2006.

[25] A. Stevens *et al.*, "Measuring soil organic carbon in croplands at regional scale using airborne imaging spectroscopy," *Geoderma*, vol. 158, no. 1–2, pp. 32–45, 2010.

[26] A. S. Abuzaid, M. A. El-Shirbeny, and M. E. Fadl, "A new attempt for modeling erosion risks using remote sensing-based mapping and the index of land susceptibility to wind erosion," *Catena*, vol. 227, p. 107130, 2023.

[27] A. M. Saleh, "Mineral Composite Assessment of Kerbala District in Iraq By Means of Remote Sensing," unpublished.

[28] V. F. Salahalden, M. A. Shareef, and Q. A. Al Nuaimy, "Characterization of the Chemical Properties of Deposited Red Clay Soil Using GIS Based Inverse Distance Weighted Method in Kirkuk City, Iraq," *Ecol. Eng. Environ. Technol.*, vol. 24, no. 7, 2023.

[29] L. S. Bernstein, X. Jin, B. Gregor, and S. M. Adler-Golden, "Quick atmospheric correction code: algorithm description and recent upgrades," *Opt. Eng.*, vol. 51, no. 11, p. 111719, 2012.

[30] M. König, M. Hieronymi, and N. Oppelt, "Application of Sentinel-2 MSI in Arctic research: Evaluating the performance of atmospheric correction approaches over Arctic sea ice," *Front. Earth Sci.*, vol. 7, p. 22, 2019.

[31] M. Saponaro, A. Agapiou, D. G. Hadjimitsis, and E. Tarantino, "Influence of spatial resolution for vegetation indices' extraction using visible bands from unmanned aerial vehicles' orthomosaics datasets," *Remote Sens.*, vol. 13, no. 16, p. 3238, 2021.

[32] L. Daniels *et al.*, "Identifying the Optimal Radiometric Calibration Method for UAV-Based Multispectral Imaging," *Remote Sens.*, vol. 15, no. 11, p. 2909, 2023.

[33] A. Al-jaf, "Remote sensing and GIS for studying some geological phenomena and mineral deposits in the western Desert in IRAQ," M.Sc. thesis, Univ. of Baghdad, 2008.

[34] S. Qiu, Z. Zhu, P. Olofsson, C. E. Woodcock, and S. Jin, "Evaluation of Landsat image compositing algorithms," *Remote Sens. Environ.*, vol. 285, p. 113375, 2023.

[35] T. Lillesand, R. W. Kiefer, and J. Chipman, *Remote Sensing and Image Interpretation*, 7th ed. Hoboken, NJ, USA: Wiley, 2015.

[36] G. Lipton and A. G. Gubins, "Spectral and microwave remote sensing: An evolution from small scale regional studies to mineral mapping and ore deposit targeting," in *Proc. Explor. 97: 4th Decennial Int. Conf. Mineral Explor.*, 1997, pp. 43–58.

[37] E. Yetkin, V. Toprak, and M. L. Süzen, "Alteration Mapping By Remote Sensing Application To Hasandağ Melendiz Volcanic Complex," unpublished.

[38] N. Ott, T. Kollersberger, and A. Tassara, "GIS analyses and favorability mapping of optimized satellite data in northern Chile to improve exploration for copper mineral deposits," *Geosphere*, vol. 2, no. 4, pp. 236–252, 2006.